Osmotic collapse of a void in an elastomer: breathing, buckling and creasing†‡

Shengqiang Cai,[a] Katia Bertoldi,*[a] Huiming Wang[ab] and Zhigang Suo*[a]

Received 29th May 2010, Accepted 12th July 2010
DOI: 10.1039/c0sm00451k

This paper studies the collapse of a void in an elastomer caused by osmosis. The void is filled with liquid water, while the elastomer is surrounded by unsaturated air. The difference in humidity motivates water molecules to permeate through the elastomer, from inside the void to outside the elastomer, leaving the liquid water inside the void in tension. When the tension is low, the void reduces size but retains the shape, a mode of deformation which we call breathing. When the tension is high, the void changes shape, possibly by two types of instability: buckling and creasing. The critical conditions for both types of instability are calculated. A tubular elastomer collapses by buckling if the wall is thin, but by creasing if the wall is thick. As the tension increases, a thin-walled tube undergoes a buckle-to-crease transition.

1. Introduction

Soft materials, such as elastomers and polymeric gels, are extensively used in biomimetic microvascular systems.[1–5] Applications include tissue scaffolds,[6] self-healing materials,[7] and microreactors.[8] A microvascular system contains channels that transport water or other liquids. In some designs, the flow in a channel can be regulated by swelling or elastic deformation of the soft materials.[9–13] The channel may collapse and open reversibly, in response to changes in environmental variables, such as a mechanical force, humidity, temperature, pH, and ionic strength.

This paper is motivated by an observation made in a study of artificial trees on chips.[1] Fig. 1 illustrates the cross section of a spherical or cylindrical void in an elastomer. The void is filled with pure liquid water, while the elastomer is surrounded by unsaturated air. The difference in humidity motivates water molecules to permeate through the elastomer, from inside the void to outside the elastomer. Consequently, the liquid water inside the void is in a state of triaxial tension. It is known that liquid water can sustain tension well in excess of 1 MPa,[14] a condition commonly found in nature in the xylem of trees.[15]

The tension inside the void causes the elastomer to deform (Fig. 2). When the tension is low, the void reduces size but retains the spherical or cylindrical shape, a mode of deformation which we call breathing. Breathing involves a field of inhomogeneous and finite deformation, and has been studied extensively.[16–20] When the tension is high, the void changes shape, possibly by two types of instability, buckling and creasing. Buckling keeps the surface of the void smooth, but creasing causes the surface of the void to self-contact.

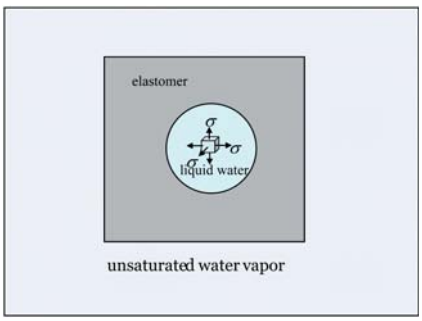

Fig. 1 A void in an elastomer is filled with pure liquid water, and the elastomer is surrounded by unsaturated water vapor. The difference in humidity motivates water molecules to permeate through the elastomer, from inside the void to the outside of the elastomer. The osmosis leaves the liquid water inside the void in a state of triaxial tension.

This paper studies the osmotic collapse, with emphasis on transitions from one type of deformation to another. Furthermore, we attempt to elucidate the distinction between buckling and creasing within the context of osmotic collapse. Both buckling and creasing set in by deviating from breathing. The natures of the small deviation, however, differ for the two types of instability. Buckling sets in when the deformation deviates from breathing by a field of strain infinitesimal in amplitude, but finite in space. By contrast, creasing sets in when the deformation deviates from breathing by a field of strain large in amplitude, but infinitesimal in space. The two types of instability are reminiscent of Gibbs's two categories of infinitesimal changes to which a metastable phase must resist. One is a change infinitesimal in degree but large in extent, and the other is a change large in degree but infinitesimal in extent.[21]

We will analyze the onset of buckling by perturbing the state of breathing with a field of infinitesimal strain. This approach, known as the linear perturbation analysis, leads to an eigenvalue problem with a spectrum of solutions.[22–28] Each solution corresponds to a mode of buckling, with the eigenvalue representing a critical value of the internal tension, and with the eigenfuntion representing a field of infinitesimal strain superimposed on the finite deformation of breathing.

We will analyze the onset of creasing by perturbing the state of breathing with creases of small lengths. The perturbed field is

[a]*School of Engineering and Applied Sciences and Kavli Institute, Harvard University, Cambridge, MA, 02138, USA. E-mail: bertoldi@seas.harvard.edu; suo@seas.harvard.edu*
[b]*Department of Mechanics, Zhejiang University, Hangzhou, 310027, Zhejiang, P. R. China*

† Electronic supplementary information (ESI) available: Finite deformation of thick-walled cylinders under internal stress and linear perturbation from a state of finite deformation. See DOI: 10.1039/c0sm00451k

‡ This paper is part of a *Soft Matter* themed issue on The Physics of Buckling. Guest editor: Alfred Crosby.

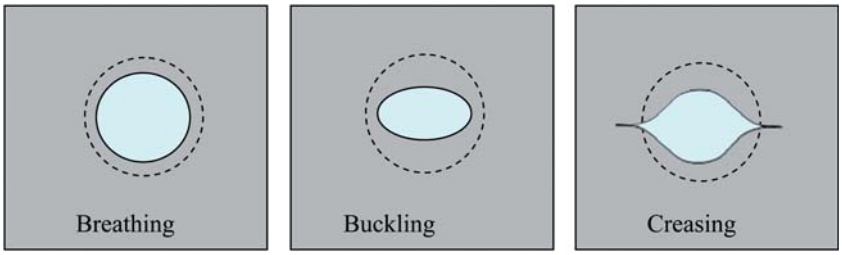

Fig. 2 The tension in the liquid water causes the elastomer to deform. Illustrated are three types of deformation: breathing, buckling, and creasing.

Fig. 3 Constrained in a bowl, a rising dough forms creases (courtesy of Michael D. Thouless).

equilibrated by using the finite element method. While creases are readily observed in daily life (*e.g.*, Fig. 3), their scientific understanding is at its beginning.[29–37] Because the initial creases are localized in space, the onset of each crease is autonomous, when a material particle reaches a critical state of strain. The set of critical states of strain can be determined, independent of specific boundary-value problems. We will ascertain this autonomy by comparing the critical condition for creasing on the curved surface of the void to that on the flat surface of a block.

We will study the transition between buckling and creasing. For a void in a large block of an elastomer, we find that the critical value of the internal tension to initiate creasing is lower than that to initiate buckling. As osmosis builds up the internal tension, the void initially shrinks but retains the cylindrical or spherical shape, and then creases set in. By contrast, for a void in an elastomer of a sufficiently small thickness, we find that the critical value of the internal tension to initiate creasing is higher than that to initiate buckling. The void buckles when the internal tension exceeds the critical value. As the internal tension increases further, the void deforms in the buckled shape, and then forms creases.

The elastomer is taken to be permeable to water molecules. As water molecules permeate out, the void reduces size, and the liquid water inside the void builds up tension. A full analysis of this process involves the kinetics of permeation. Attention in this paper will be restricted to the state of equilibrium, when the chemical potential of water has equalized between the liquid water inside the void and the water vapor outside the elastomer. Furthermore, we will neglect swelling of the elastomer due to the absorption of water. This simplification may be justified in practice, because the magnitude of the internal tension is relatively high, and elastomers used in experiments are often heavily crosslinked.

2. Tension in liquid water caused by osmosis

With reference to Fig. 1, in equilibrium, the tension in the liquid water inside the void can be related to the humidity outside the elastomer by the method of thermodynamics. When liquid water equilibrates with its own vapor, in the absence of any other species of molecules, the pressure in the coexistent liquid and vapor is denoted by p_0. (At room temperature, $p_0 = 3.2$ kPa.) The coexistent liquid and vapor are taken as the state of reference, in which the chemical potential of water is set to be zero. We next list the chemical potentials of water in several idealized systems.

The air outside the elastomer has several molecular species, and is modeled as an ideal gas. The chemical potential of water in the gas is

$$\mu = kT\log(p/p_0) \tag{1}$$

where kT is the temperature in the unit of energy, and p the partial pressure of water molecules in the gas. The ratio p/p_0 defines the relative humidity of the gas.

For a gas in a closed environment, the relative humidity can be set by placing in the environment an aqueous solution. In a dilute aqueous solution, the chemical potential of water is given by the van't Hoff equation:

$$\mu = -\Omega ckT \tag{2}$$

where Ω is the volume per water molecule ($\Omega = 3.0 \times 10^{-29}\mathrm{m}^3$), c is the concentration of the solution (*i.e.*, the number of solute particles per unit volume of the solution). When the gas equilibrates with the solution, the chemical potential of water in the gas equals that in the solution. A comparison of (1) and (2) relates the partial pressure of water in the gas to the concentration of the solution.

When pure liquid water is subject to a triaxial stress σ, the chemical potential of water is

$$\mu = -\Omega(\sigma + p_0) \tag{3}$$

We adopt the sign convention that the stress in the liquid water is a tension if $\sigma > 0$, and is a pressure if $\sigma < 0$. Eqn (3) recovers the state of reference: the chemical potential vanishes when $\sigma = -p_0$. Often the magnitude of the vapor pressure p_0 is negligible compared to the magnitude of the stress σ in the liquid water, so that we may drop p_0 from (3).

When the pure liquid water inside the void equilibrates with the water molecules in the gas outside the elastomer, the chemical potential of water equalizes. A comparison of (1)–(3) gives the tension in the liquid water inside the void:

$$\sigma = \frac{kT}{\Omega}\log\left(\frac{p_0}{p}\right) = ckT \tag{4}$$

For example, the tension in the liquid water inside the void is $\sigma = 1$ MPa when the relative humidity outside the elastomer is $p/p_0 = 99.3\%$, or when the concentration of the aqueous solution is $c = 0.4$M.

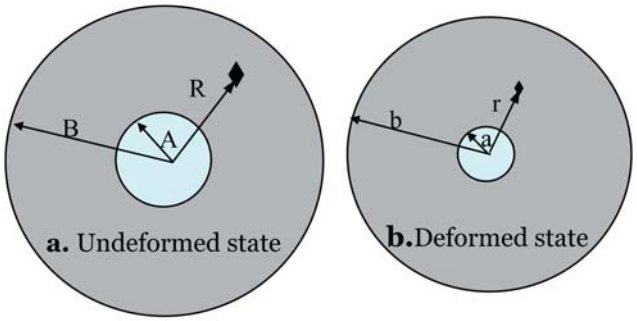

3. Breathing

This section assumes that the elastomer deforms by either spherical or cylindrical symmetry (*i.e.*, the breathing mode). As mentioned in the Introduction, we consider the state of equilibrium and neglect the swelling of the elastomer. Consequently, the phenomenon reduces to a void in an incompressible solid subject to traction on the surface of the void. Boundary-value problems for both cylindrical and spherical voids have been solved analytically,[16] and used to interpret cavitation in soft materials.[17–20] We list the governing equations in Appendix A (ESI†), and discuss the results here within the context of osmotic collapse.

Fig. 4 illustrates a cross section of a void in an elastomer of spherical or cylindrical symmetry. When the elastomer is undeformed, the radius of the void is A, and the external radius of the elastomer is B. When the elastomer is deformed, the radius of the void becomes a, and the external radius of the elastomer becomes b. For the time being, the thickness of the elastomer is taken to be much larger than the radius of the void, $B/A \to \infty$. For the cylindrical void, the elastomer is taken to deform under plane-strain conditions, and the stress σ inside the cylindrical void relates to the radius a of the void as

$$\frac{\sigma}{G} = -\frac{1}{2} + \frac{1}{2}\left(\frac{a}{A}\right)^{-2} - \log\frac{a}{A} \tag{5}$$

For a spherical void, the relation is

$$\frac{\sigma}{G} = -\frac{5}{2} + 2\left(\frac{a}{A}\right)^{-1} + \frac{1}{2}\left(\frac{a}{A}\right)^{-4} \tag{6}$$

Fig. 4 shows the normalized stress in the void, σ/G, as a function of the stretch of the void, a/A. The void enlarges when the water inside the void is under pressure, and the void shrinks when the water inside the void is under tension.

The curves for the cylindrical void and the spherical void look similar, but differ in some details. For the cylindrical void, $\sigma/G \to -\infty$ as $a/A \to \infty$. By contrast, for the spherical void, $\sigma/G \to -5/2$ as $a/A \to \infty$. Consequently, the spherical void enlarges indefinitely when the internal pressure reaches a critical value, known as the cavitation limit. This difference between the cylindrical and spherical void, however, may not be pronounced in practice. The elastomer is a network of polymer chains, and stiffens steeply when the polymer chains are stretched near their contour lengths. The steep stiffening is not represented by the neo-Hookean material model, which is used to obtain the solutions (5) and (6). Once the steep stiffening is considered, for both the cylindrical and spherical voids, the magnitude of the internal pressure will increase without limit as the voids expand. Fig. 4 does illustrate a qualitative trend: the voids can expand substantially for modest increase in the internal pressure.

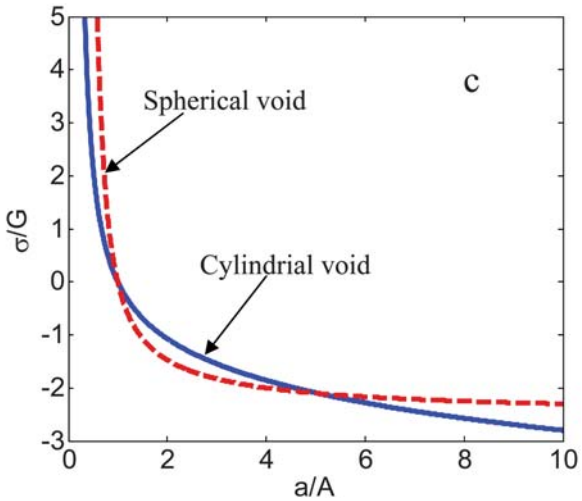

Fig. 4 Under internal stress, the void changes size but retains shape, a mode of deformation which we call breathing. (a) Undeformed state. (b) Deformed state. (c) Normalized stress inside the void as a function of the normalized radius of the void ($B/A \to \infty$).

Of more relevance to the present work is when the water inside the voids is under tension. As shown in Fig. 4, for both the spherical and the cylindrical voids, the internal tension rises steeply as the voids shrink. The breathing mode of deformation may be used to estimate the shear modulus of the elastomer. For example, for a pHEMA gel with crosslinker of 6 v% EGDMA, the experiment showed that a spherical void shrank by $a/A = 0.71$ when the relative humidity was 0.98 outside the elastomer; see Fig. 2(B) of ref. 1. According to (4), this relative humidity induces in the liquid water inside the void a tension of $\sigma = 2.8$ MPa. Reading from Fig. 4, a stretch of $a/A = 0.71$ corresponds to $\sigma/G = 2.3$. Consequently, the shear modulus of the elastomer is estimated to be $G = 1.2$ MPa. Unfortunately, the value of the shear modulus was not reported in the original paper.

Observe that the stress-stretch curves in Fig. 4 are steep when the water is in tension, and are much less steep when the water in compression. Consequently, more accurate determination of the modulus of the elastomer is possible by observing an expanding void under internal pressure. Indeed, a technique in which

pressurized water is injected into a soft material by a syringe has been developed recently.[18] The pressure in water can also be induced by osmosis, when the void contains a concentrated aqueous solution, imbibing water from outside the elastomer.

4. Buckling

When the tension in the liquid water inside the void is high, the deformation of cylindrical or spherical symmetry becomes unstable. This section considers one type of instability, buckling, which can be analyzed by the method of linear perturbation analysis.[22–28] Implementation of this method for the cylindrical void is summarized in Appendix B (ESI†). Here we discuss the main results.

In the limit that the buckling wavelength is much smaller than the radius of the void, the critical condition for buckling is unaffected by the curvature of the void. The buckling of a flat surface of a semi-infinite block was analyzed by Biot.[22] Before buckling, the block is in a state of homogeneous and finite deformation, of principal stretches λ_1, λ_2 and λ_3. When this state is perturbed by a field of infinitesimal strain, the resulting inhomogeneous state is also a state of equilibrium, and the perturbation is required to be localized to the surface of the block. Any such a field of infinitesimal strain is a linear superposition of a set of eigenfields, each of which is sinusoidal, with the wavevector pointing in a direction parallel to the surface, and the amplitude decaying exponentially in the direction normal to the surface. Because the semi-infinite block offers no length to the boundary-value problem, the eigenfields can be of any wavelength, and the wavelength does not affect the critical condition. Biot's analysis gave the critical condition for buckling:

$$\lambda_3/\lambda_1 = 3.383 \tag{7}$$

Here direction 3 is normal to the surface of the block, and direction 1 coincides with that of the wave vector of the sinusoidal perturbation. The critical condition is valid under the generalized plane-strain condition, where λ_2 is constant in the block, but need not be the unity. The three principal stretches satisfies the condition of incompressibility, $\lambda_1\lambda_2\lambda_3 = 1$.

On the surface of the cylindrical void under the plane-strain conditions, $\lambda_z = 1$, $\lambda_\theta = a/A$, and $\lambda_r = (a/A)^{-1}$. Consequently, we can specialize Biot's condition (7), giving the critical condition in terms of the stretch of the void, $a/A = 0.5437$. Inserting this critical stretch into (5), we obtain $\sigma_{cr} = 1.801G$, the critical value of the internal tension for the cylindrical void to buckle.

The surface of the spherical void is under stretches $\lambda_1 = \lambda_2 = a/A$ and $\lambda_3 = (a/A)^{-2}$. Consequently, we can specialize Biot's condition (7), giving the critical condition in terms of the stretch of the void, $a/A = 0.6661$. Inserting this critical stretch into (6), we obtain $\sigma_{cr} = 3.042G$, which is the critical condition for the spherical void to buckle.

We next discuss the effects of the ratio B/A and the mode number m. When the wavelength of perturbation is small compared to the radius of the void, the effect of the curvature of the void is negligible, and Biot's solution of wrinkling of flat surface should apply. Inserting $a/A = 0.5437$ into (A1) and (A6), we obtain the critical stress inside the void as a function of B/A. This function is plotted as a dashed line in Fig. 5a. When the wavelength of perturbation is comparable to the radius of the void, the critical condition depends on the mode of buckling, m. This critical condition is obtained by numerical integration of the eigenvalue problem described in Appendix B (ESI†). Fig. 5a shows the critical stress for the cylindrical tube for several values of m. As expected, Biot's limit is approached when $m \to \infty$. (Observe that the difference between Biot's limit and the numerical results for $m = 100$ is within 1.5%.) The critical stress for the onset of buckling of each mode increases with the thickness of the tube, approaching an asymptotic value as $B/A \to \infty$.

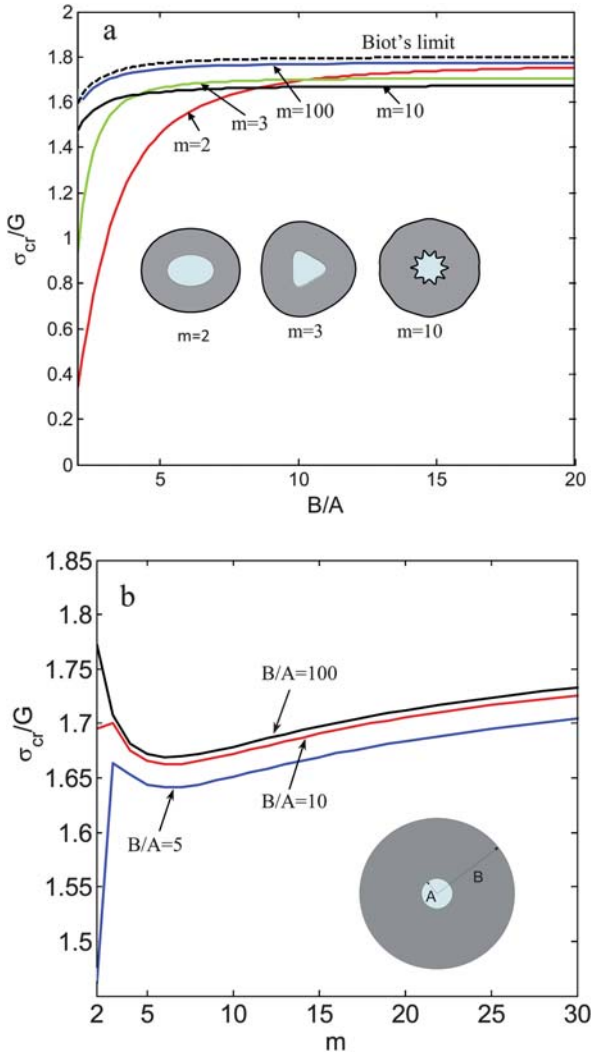

Fig. 5 (a) Critical tension as a function of B/A for $m = 2$, 3, 10 and 100. (b) Critical tension for case $B/A = 5$, 10, 100 as a function of the mode number m.

Fig. 5b plots the critical stress as a function of m at several values of B/A. For a tube with $B/A < 8$, the critical tension for buckling is lowest when $m = 2$. For a thicker tube (*e.g.*, $B/A = 10$ and $B/A = 100$), the critical tension for buckling is lowest when $m = 6$. These results indicate that, for a given value of B/A, the expected mode number m for buckling is finite. As will be shown in Fig. 11, however, for a tube with $B/A > 3$, a different type of instability, creasing, sets in at a stress lower than that for

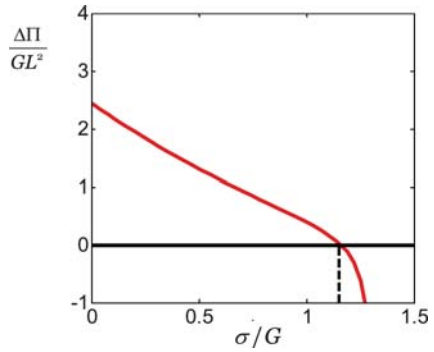

Fig. 6 The difference in the free energy between the creased state and the axisymmetric state.

buckling. Consequently, here we will not pursue the dependence of the critical stress on buckling mode any further.

5. Creasing

When a block of an elastomer is bent, the compressed surface remains smooth initially, but then suddenly forms a crease.[29–34] Similar creases have also been observed when a gel swells under constraint.[35–38] As mentioned before, buckling and creasing are different types of instability. Buckling sets in when the deformation deviates from breathing by a field of strain infinitesimal in amplitude, but finite in space. By contrast, creasing sets in when the deformation deviates from breathing by a field of strain finite in amplitude, but infinitesimal in space.

Consider a semi-infinite block in a homogeneous state of finite deformation, of principal stretches λ_1, λ_2 and λ_3. The critical condition for the onset of a crease of the surface of the is[34]

$$\lambda_3/\lambda_1 = 2.4 \tag{8}$$

Here direction 3 is normal to the surface of the block, and direction 1 is in the surface and normal to the crease. The critical condition is valid under the generalized plane-strain condition, where λ_2 is constant in the block, but need not be the unity. The three principal stretches satisfies the condition of incompressibility, $\lambda_1\lambda_2\lambda_3 = 1$.

Because the initial creases are localized in space, each initial crease is autonomous. Consequently, the critical condition (8) is expected to be applicable to the onset of a crease on the surface of an elastomer of any shape. On the surface of the cylindrical void, before a crease sets in, the principal stretches are $\lambda_1 = a/A$, $\lambda_2 = 1$, and $\lambda_3 = (a/A)^{-1}$. Consequently, the critical condition (8) gives $a/A = 0.65$. Inserting this critical stretch into (5), we obtain $\sigma_{cr} = 1.12G$, the critical condition for the onset of creasing for the cylindrical void.

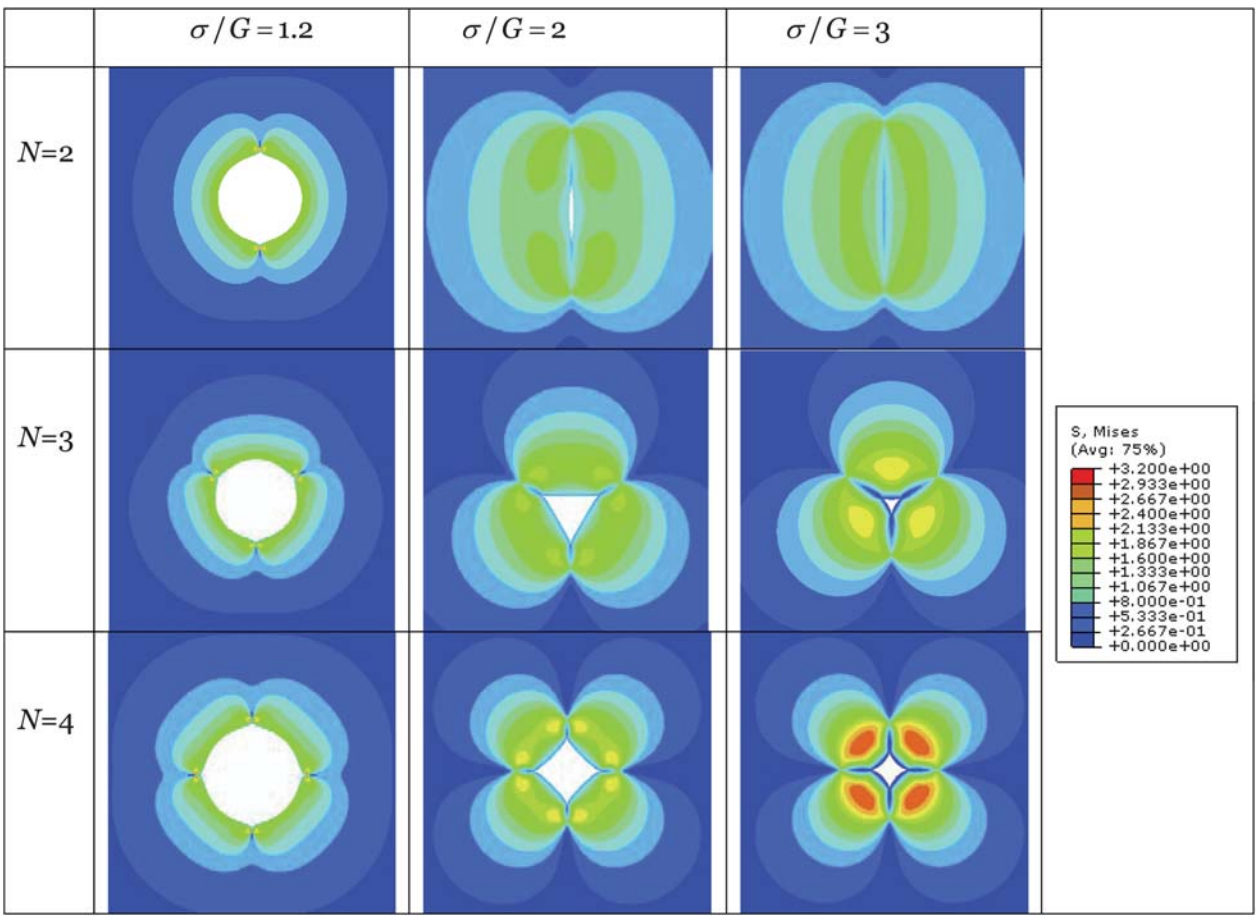

Fig. 7 As the tension in the liquid water inside the void increases, the field of deformation in the elastomer evolves. The number of creases, N, is prescribed in the beginning of the simulation. The color indicates the level of the von Mises stress.

On the surface of the spherical void, before a crease sets in, the principal stretches are $\lambda_1 = \lambda_2 = a/A$ and $\lambda_3 = (a/A)^{-2}$. Consequently, the critical condition (8) gives $a/A = 0.75$. Inserting this critical stretch into (6), we obtain $\sigma_{cr} = 1.75G$, the critical condition for the onset of creasing for the spherical void. Creases of an initially spherical void have been reported; see Fig. 2B of ref. 1. The reported experimental details, however, are insufficient to be compared to theoretical predications.

To illustrate the autonomy of the onset of individual creases, we analyze creases on the surface of the cylindrical void by using the finite element code ABAQUS. In the calculation, the elastomer is represented by a tube, of inner radius A and outer radius B. We consider the onset of two creases on the surface of the void, as illustrated in Fig. 2. Symmetry is assumed such that only a quarter of the elastomer is simulated. Following an approach described in ref. 34, we introduce a crease of length L by prescribing the displacements of the creased region as boundary conditions. To study the onset of creasing, the length of crease is set to be small compared to the radius of the void, say, $L/A = 1/20$. The inner surface of the elastomer is prescribed with the uniform tension σ normal to the surface, and the outer surface is traction-free. In the calculation, we use elements of type CPE6MH. The free energy of the system Π consists of the elastic energy of the elastomer and the potential energy due to the prescribed internal tension. Dimensional analysis indicates that the free energy per unit thickness of the creased elastomer minus that of the axisymmetrically deformed body should take the form

$$\Delta\Pi = GL^2 f\left(\frac{\sigma}{G}\right) \tag{9}$$

The dimensionless function $f(\sigma/G)$ is obtained by using ABAQUS, and is plotted in Fig. 6. The outer radius is varied in the calculation, and the results shown in Fig. 6 are for $B/A = 20$. The numerical result shows that the creased body has a lower free energy than the smooth body when $\sigma > 1.12G$. This result reproduces the critical stress estimated above.

After the creases set in, as the internal tension increases, the elastomer deforms further. Fig. 7 shows the shape of the void at several levels of internal tension. The color indicates the level of the von Mises stress. The calculation starts with a number of prescribed small creases of a small length. We use ABAQUS to evolve the field of deformation in the elastomer as the internal tension σ increases. Fig. 8 plots the length of the creases and the area of the void as functions of the internal tension. A void with two creases is particularly effective in reducing its area. In practice, the change in the area of the void can be used to regulate vascular transport.

For a void of a perfect cylindrical shape, the state of deformation is the same at every material particle on the surface of the void. Consequently, creases may set in anywhere on the surface of the void when the tension inside the void exceeds the critical value, $\sigma_{cr} = 1.12G$. When the length of each crease is much smaller than the radius of the void, the fields associated with individual creases are autonomous, and do not overlap with one another. Every crease reduces the free energy of the system, so that a larger number of creases will reduce more energy. When the length of each crease goes beyond some fraction of the radius of the void, the fields associated with individual creases are no longer autonomous, but overlap with one another.

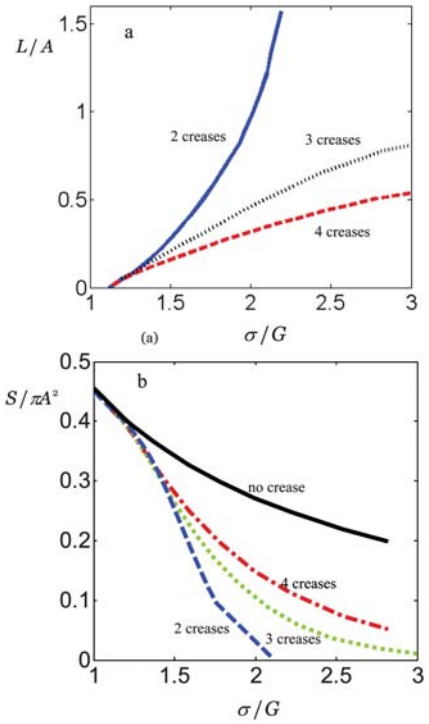

Fig. 8 The length (a) of the creases and the cross-sectional area (b) of the void change with the internal tension, as well as with the number of creases.

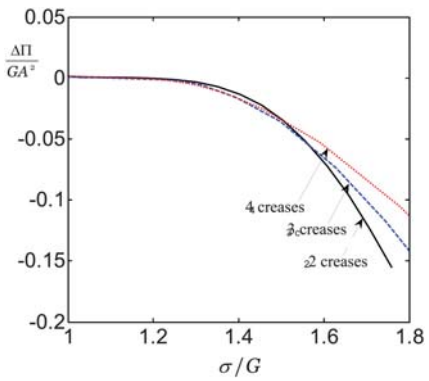

Fig. 9 The difference in the free energy between the creased state and the axisymmetric state.

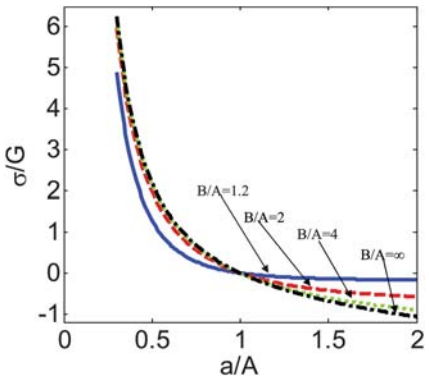

Fig. 10 Stress in the cylindrical void as a function a/A for several values of B/A.

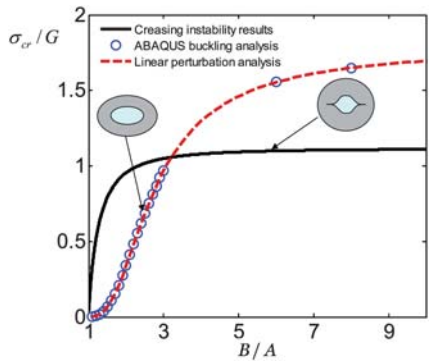

Fig. 11 Buckling-to-creasing transition. The elastomer is a cylindrical shell, with inner radius A and outer radius B in the undeformed state. A thin shell buckles, and a thick shell creases.

Consequently, some intermediate number of creases will minimize the free energy of the system.

Fig. 9 plots the free energy of a creased body minus that of a smooth body as a function of the internal tension. When the internal tension is slightly above σ_{cr}, the body with more creases has slightly lower potential energy. When the internal tension is beyond some level, the body with two creases has the lowest potential energy. It is likely that multiple creases set in when the internal tension exceeds the critical value, but the number of creases reduces to two when the internal tension is high.

6. Buckle-to-crease transition

As described in the previous two sections, for a cylindrical void in a large block of an elastomer, buckling of mode $m = \infty$ sets in at the critical tension $\sigma_{cr}/G = 1.801$, and creasing sets in at the critical tension $\sigma_{cr}/G = 1.12$. Fig. 5 shows that, for large values of B/A, the critical tension for all modes of buckling exceeds that for creasing. Consequently, when the radius of the void is small compared to the size of the elastomer, the void will collapse by creasing.

Also evident in Fig. 5 is that, the critical tension for buckling reduces for small values of B/A. This trend is readily understood: a tube of a thin wall buckles at a lower tension than that of a thick wall. As the internal tension increases, will a thin-walled tube buckle before crease? Appendix A (ESI†) derives the deformation of the breathing mode for a tube under internal stress. Fig. 10 shows the internal tension as a function of the stretch of the void for various values of B/A. As expected, thin-walled tubes are more deformable. Because the onset of each crease is autonomous, independent of the thickness of the wall, the crease sets in at the critical stretch $a/A = 0.65$. This critical stretch, together with Fig. 10, determines the critical tension for the onset of creasing for a thick-walled tube. Fig. 11 compares the critical conditions for buckling and creasing. When B/A is large, the critical tension for creasing is lower than that for buckling, and the void is expected to collapse by creasing. When B/A is small, the critical tension for buckling is lower than that for creasing, and the void is expected to collapse by buckling.

After the elastomer buckles, the surface of the void remains smooth as the internal tension increases. However, when a tip of the buckle is compressed beyond a critical level, the surface may form a crease. Fig. 12 shows two sequences of finite-element simulation. In both sequences, the tube buckles prior to creasing. For $B/A = 1.2$, the buckled tube first self-contacts in the middle of the wall, and then creases form at the two tips. For $B/A = 1.6$, the buckled tube creases prior to the self-contact in the middle.

The transition between buckling and creasing may be quite common in practice. A recent example involves a layer of a hydrogel attached to a rigid substrate.[38,39] The hydrogel contains a lattice of cylindrical holes. When the hydrogel swells in a solvent, each cylindrical hole collapses by buckling first, and creases form when the hydrogel swells further. A second example involves a stiff film attached to a compliant substrate.[40,41] When the substrate is compressed, the film first form periodic wrinkles. As the compressive strain increases, some of the wrinkles deepen and self-contact.

7. Concluding remarks

For a water-filled void in an elastomer, the water inside the void can be in tension due to osmosis, causing the elastomer to

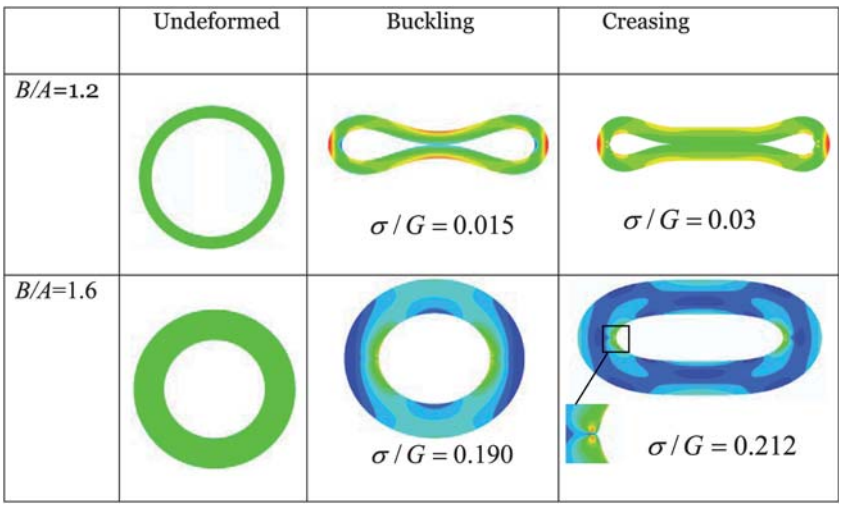

Fig. 12 As the internal tension increases, the tube may buckle first, and then crease.

deform. As the tension builds up, the void reduces the size, but the shape of the void initially remains unchanged, a mode of deformation which we call breathing. When the tension is sufficiently high, the shape of the void changes by buckling or creasing. Buckling deviates from breathing by a field infinitesimal in amplitude but large in extent, and creasing deviates from breathing by a field large in amplitude but infinitesimal in extent. A tubular elastomer collapses by creasing if the wall is thick, but collapses by buckling if the wall is thin. In the latter case, as the internal tension increases, the buckled void can deform further, leading to the formation of creases. While transitions between the three types of deformation—breathing, buckling, and creasing—may be readily observed in nature and in engineering, the scientific understanding of these transitions requires further experimental and theoretical exploration.

Acknowledgements

This work is supported by the NSF through a grant on Soft Active Materials (CMMI–0800161), by the MURI through a contract on Adaptive Structural Materials (W911NF-09-1-0476), and by the Kavli Institute at Harvard University. H.M.W. is supported by Zhejiang University through the Xinxing Plan as a visiting scholar at Harvard University, and by the National Natural Science Foundation of China (Grant No. 10872179).

References

1 T. D. Wheeler and A. D. Stroock, *Nature*, 2008, **455**, 208–212.
2 X. Noblin, L. Mahadevan, I. Coomaraswamy, D. Weitz, N. Holbrook and M. Zwieniecki, *Proc. Natl. Acad. Sci. U. S. A.*, 2008, **105**, 9140–9144.
3 D. Huh, K. Mills, X. Zhu, M. Burns, M. Thouless and S. Takayama, *Nat. Mater.*, 2007, **6**, 424–428.
4 M. Cabodi, N. Choi, J. Gleghorn, C. Lee, L. Bonassar and A. Stroock, *J. Am. Chem. Soc.*, 2005, **127**, 13788.
5 D. Therriault, S. White and J. Lewis, *Nat. Mater.*, 2003, **2**, 265–271.
6 M. Ford, J. Bertram, S. Hynes, M. Michaud, Q. Li, M. Young, S. Segal, J. Madri and E. Lavik, *Proc. Natl. Acad. Sci. U. S. A.*, 2006, **103**, 2512–2517.
7 K. Toohey, N. Sottos, J. Lewis, J. Moore and S. White, *Nat. Mater.*, 2007, **6**, 581–585.
8 M. Runyon, B. Johnson-Kerner and R. Ismagilov, *Angew. Chem., Int. Ed.*, 2004, **43**, 1531–1536.
9 D. J. Beebe, J. S. Moore, J. M. Bauer, Q. Yu, R. H. Liu, C. Devadoss and B. H. Jo, *Nature*, 2000, **404**, 588–590.
10 L. Dong, A. K. Agarwal, D. J. Beebe and H. R. Jiang, *Nature*, 2006, **442**, 551–554.
11 A. Baldi, Y. Gu, P. E. Loftness, R. A. Siegel and B. Ziaie, *J. Microelectromech. Syst.*, 2003, **12**, 613–621.
12 M. E. Harmon, M. Tang and C. W. Frank, *Polymer*, 2003, **44**, 4547–4556.
13 I. Tokarev and S. Minko, *Soft Matter*, 2009, **5**, 511–524.
14 F. Caupin and E. Herbert, *C. R. Phys.*, 2006, **7**, 1000–1017.
15 N. M. Holbrook and M. A. Zwieniecki, *Phys. Today*, 2008, **61**, 76–77.
16 R. F. Bishop, R. Hill and N. F. Mott, *Proc. Phys. Soc.*, 1945, **57**, 147–159.
17 A. N. Gent, *Rubber Chem. Tech.*, 1991, **63**, G49–G53.
18 S. Kundu and A. J. Crosby, *Soft Matter*, 2009, **5**, 3963–3968.
19 J. Dollhofer, A. Chiche, V. Muralidharan, C. Creton and C. Y. Hui, *Int. J. Solids Struct.*, 2004, **41**, 6111–6127.
20 O. Lopez-Pamies, iMechanica, Journal Club, May 2010. http://imechanica.org/node/8131.
21 J. W. Gibbs, *Collected Works*. Longmans, Green, and Co, 1906, pp. 105–115, 252–258.
22 M. A. Biot, *Appl. Sci. Res., Sect.*, 1963, **A12**, 168–182.
23 A. S. D. Wang and A. Ertepinar, *Int. J. Nonlinear Mech.*, 1972, **7**, 539–555.
24 D. M. Haughton and R. W. Ogden, *J. Mech. Phys. Solids*, 1979, **27**, 489–512.
25 J. L. Bassani, D. Durban and J. W. Hutchinson, *Math. Proc. Cambridge Philos. Soc.*, 1980, **87**, 339–356.
26 M. Ben Amar and P. Ciarletta, *J. Mech. Phys. Solids*, 2010, **58**, 935–954.
27 C. D. Coman and M. Destrade, *Q. J. Mech. Appl. Math.*, 2008, **61**, 395–414.
28 S. Roccabianca, M. Gei and D. Bigoni, *IMA J. Appl. Math.*, 2010, **75**, 525–548.
29 A. N. Gent and I. S. Cho, *Rubber Chem. Technol.*, 1999, **72**, 253–262.
30 A. Ghatak and A. L. Das, *Phys. Rev. Lett.*, 2007, **99**, 076101.
31 M. Destrade, M. D. Gilchrist, J. A. Motherway and J. G. Murphy, *Mech. Mater.*, 2010, **42**, 469–476.
32 E. B. Hohlfeld, Ph.D. thesis, Harvard University, 2008.
33 E. B. Hohlfeld and L. Mahadevan, unpublished.
34 W. Hong, X. H. Zhao and Z. G. Suo, *Appl. Phys. Lett.*, 2009, **95**, 111901.
35 V. Trujillo, J. Kim and R. C. Hayward, *Soft Matter*, 2008, **4**, 564–569.
36 J. W. Kim, J. W. Yoon and R. C. Hayward, *Nat. Mater.*, 2010, **9**, 159–164.
37 M. K. Kang and R. Huang, *Swell induced surface instability of confined hydrogel layers on substrates*, DOI: 10.1016/j.jmps.2010.07.008.
38 Y. Zhang, E. A. Matsumoto, A. Peter, P. C. Lin, R. D. Kamien and S. Yang, *Nano Lett.*, 2008, **8**, 1192–1196.
39 J. H. Jang, C. Y. Koh, K. Bertoldi, M. C. Boyce and E. L. Thomas, *Nano Lett.*, 2009, **9**, 2113–2119.
40 L. Pocivavsek, R. Dellsy, A. Kern, S. Johnson, B. H. Lin, K. Y. C. Lee and E. Cerda, *Science*, 2008, **320**, 912–916.
41 P. M. Reis, F. Corson, A. Boudaoud and B. Roman, *Phys. Rev. Lett.*, 2009, **103**, 045501.
42 K. A. Lindsay and C. E. Rooney, *J. Comput. Phys.*, 1992, **103**, 472–477.